Available online at www.sciencedirect.com

ScienceDirect

Energy Procedia 8 (2011) 527–532

Energy Procedia

SiliconPV: 17-20 April 2011, Freiburg, Germany

Accurate modeling of aluminum-doped silicon

Marc Rüdiger[a], Michael Rauer, Christian Schmiga, Martin Hermle and Stefan W. Glunz

Fraunhofer Institute for Solar Energy Systems ISE, Heidenhofstr. 2, 79110 Freiburg, Germany

Abstract

We present a detailed study on accurate modeling of highly aluminum-doped p^+ silicon. We have analyzed the influence of defect recombination and the effect of incomplete ionization on the saturation current densities of Al-p^+ regions featuring different Al doping profiles. Very good agreement within a broad range of experimental data has been obtained. We demonstrate that incomplete ionization has a significant impact on the doping profile characteristics and, therefore, has to be accounted for in accurate modeling of highly aluminum-doped silicon.

Keywords: silicon; defects; aluminum; incomplete ionization

1. Introduction

Highly aluminum-doped p^+ silicon is commonly used as back surface fields (BSFs) in p-type Si solar cells. Its easy formation by alloying of screen-printed Al pastes during a short high-temperature firing step is a reliable low-cost process and is thus, implemented in most industrial photovoltaic production lines. Such Al-p^+ regions can also be applied as rear emitters to n-type Si solar cells, which is a promising topic of current research [1-9].

In device simulations, saturation current densities j_0 of Al-doped Si are calculated too low if Al atoms are considered to be acceptor occupancies, in analogy to the description of boron acceptors, as usually done by the simulation tool PC1D [10]. This leads to significantly overestimated open-circuit voltages V_{oc}. Recently, for simulation purposes, a minority carrier lifetime parameterization as a function of the Al acceptor density N_A has been reported [11]. This model empirically accounts for the lifetime limiting defect in Al-doped Si, which may be caused by the formation of aluminum-oxygen (Al-O) defect

a) Corresponding author. Tel.: +49-761-4588-5921; fax: +49-761-4588-9250.
E-mail address: marc.ruediger@ise.fraunhofer.de.

1876–6102 © 2011 Published by Elsevier Ltd. Selection and/or peer-review under responsibility of SiliconPV 2011.
Open access under CC BY-NC-ND license. doi:10.1016/j.egypro.2011.06.177

complexes [12-15]. However, we show that the current models are not suitable for describing highly Al-doped Si in good accordance within a broad range of experimental data.

Thus, in this work, we analyze the effect of Auger and Shockley-Read-Hall (SRH) recombination [16, 17] on the saturation current densities j_0 of surface-passivated and non-surface-passivated Al-doped p^+ Si (Al-p^+) regions. Thereby, we demonstrate that an additional effect has a major impact on the behavior of Al-doped Si, which we have identified as incomplete ionization of the Al acceptor atoms. We show that the effect of incomplete ionization of Al acceptors is an important mechanism in Al-doped Si and has to be accounted for in accurate solar cell modeling.

2. Experimental data base and simulation setup

We have prepared a broad range of test samples on high-quality 100 Ωcm boron-doped p-type float-zone (FZ) Si material. These samples hold Al-p^+ regions, differing in depth and surface passivation and have been characterized in detail elsewhere [18, 19]. One part of the samples features non-passivated, whereas the second part exhibits effectively passivated Al-doped p^+ Si surfaces. For passivation, we used atomic-layer-deposited aluminum-oxide (Al_2O_3) or plasma-enhanced-chemical-vapor-deposited amorphous Si (a-Si) layers. To obtain the doping profiles, the total Al concentrations (ionized and non-ionized Al atoms) have been measured by the electrochemical capacitance-voltage (ECV) method. Further experimental proof for measuring the total Al concentration will be published soon. The opposite non-Al-doped sample surfaces are passivated by silicon-nitride (SiN_x), leading to an asymmetric structure, as shown schematically in Fig. 1. We have determined the saturation current densities $j_{0,Al}$ of the Al-p^+ regions [20] via quasi-steady-state photoconductance (QSSPC) measurements [21]. The experimentally obtained $j_{0,Al}$ values of different Al-p^+ regions are summarized in Fig. 1 (squares).

For the numerical determination of the saturation current densities $j_{0,Al}$ via one-dimensional simulations, we have set up an asymmetric sample structure, equivalent to the experiment, in Sentaurus TCAD [22]. In order to calculate the current density-voltage characteristic of the device, a very thin and shallow phosphorus-doped n^+ emitter on the front was assumed, holding negligible Auger recombination. Furthermore, we have implemented a non-recombining front contact and a rear contact with adjustable surface recombination velocity. From the short-circuit current density j_{sc} and the open-circuit voltage V_{oc},

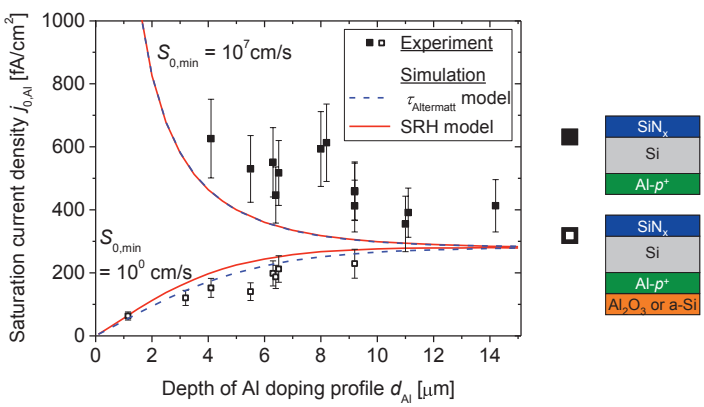

Fig. 1. Measured saturation current densities $j_{0,Al}$ of our test samples featuring non-passivated (solid squares) and passivated (open squares) Al-p^+ surfaces. The curves show calculations for SRH recombination with $N_t^* = 1.7$ cm^{-1} (named as SRH model) and the lifetime parameterization ($\tau_{Altermatt}$ model) proposed in Ref. [11], applying a generalized profile for depth variations.

the saturation current density $j_{0,Al}$ can be calculated via the one-diode equation. Thereby, the influences of j_0 of the bulk and the front side emitter can be neglected.

As obtained by ECV measurements (Fig. 2), the Al doping profile curve starts at a concentration of approx. 1×10^{18} cm^{-3} at the surface, rising to a maximum value of ~ 3×10^{18} cm^{-3} at a depth of some μm (typical depths are in the range from 5 to 8 μm in solar cells), where it decreases rapidly. At the interface of the Al-doped p^+ Si and the Si bulk, the profile is broadly blurred due to lateral thickness inhomogeneities of the Al-p^+ region. Scanning electron microscope (SEM) images indicate an abrupt profile decrease due to a sharp potential contrast between the Al-doped Si layer and the Si base [18, 19]. Thus, the measured Al doping profiles have been fitted by a convolution of an abrupt profile, which acts finally as the profile for the simulations, and a Gaussian distribution [20, 23].

For depth variations, we set up a generalized Al doping curve based on the deconvoluted abrupt profile, consisting of an exponential increase from $N_A = 1\times10^{18}$ cm^{-3} at the surface to $N_A = 3\times10^{18}$ cm^{-3} at the Al-p^+/Si interface and an abrupt decay at the depth d_{Al} of the Al doping profile. Device modeling has been carried out at an intrinsic carrier concentration of 9.65×10^9 cm^{-3} [24, 25].

3. Comparison of defect models

Al and Al-related defect centers form electrically active deep energy levels near the Si mid-gap, leading to high recombination and, thus, to detrimental consequences for the minority carrier lifetime. The carrier lifetime limiting defect in Al-doped Si may be related to Al-O defect complexes [12-15].

Recently, for simulation purposes, a minority carrier lifetime parameterization $\tau_{Altermatt}/\mu s = ((N_A/cm^{-3})^{1.5048}\cdot 2.8339\times10^{-24}\cdot f)^{-1}$ as a function of the Al acceptor density N_A has been reported [11] with the dimensionless scaling factor $f = 2\times10^{-3}$ [26]. This parameterization is based on Shockley-Read-Hall (SRH) theory [16, 17] and is referred to as $\tau_{Altermatt}$ model.

For defect modeling via SRH theory, which is the general description of carrier generation and recombination at a single defect level, the entire defect parameter set consisting of defect energy E_t, the capture cross sections for electrons and holes $\sigma_{e/h}$, respectively, and the defect concentration N_t is required. The SRH minority carrier lifetime equals the minority carrier capture time constant $\tau_{n0} \equiv (N_t\cdot\sigma_e\cdot v_{th,e})^{-1}$ under low-level injection (LLI) conditions. $v_{th,e}$ is the thermal velocity of electrons. Since the value of σ_e is based on a rare data base from literature [12, 13] and the defect density N_t is unknown, the product of these two values has been defined as the effective defect density $N_t^*(N_A) \equiv N_t(N_A)\cdot\sigma_e$, acting as a free parameter in our simulations. Thereby, as a first order approximation, N_t is proportional to N_A. Thus, Al-doped Si can be described without exact knowledge of the correct set of defect parameters for the Al-O complex. Please note that N_t^* indicates the effective defect density at the maximum acceptor concentration $N_t^*(N_{A,max}) = N_t^*(3\times10^{18}\ cm^{-3})$. However, to determine the absolute defect concentration N_t, the knowledge of the minority carrier capture cross section σ_e is required.

For comparison, we have carried out simulations applying the $\tau_{Altermatt}$ model and the SRH model, in combination with the generalized Al doping profiles (cf. section 2). The results for the calculated $j_{0,Al,Altermatt}$ (dashed) and $j_{0,Al,SRH}$ (solid/continuous) curves are shown in Fig. 1. Thereby, $N_t^* = 1.7$ cm^{-1} has been chosen according to the $j_{0,Al,Altermatt}$ value at the convergence limit for very thick Al doping profiles with $d_{Al} \geq 15$ μm. As both approaches depict a very similar structure, a good correlation between $j_{0,Al,SRH}$ (with $N_t^* = 1.7$ cm^{-1}) and $j_{0,Al,Altermatt}$ is achieved, especially for non-surface-passivated Al-doped Si. For passivated Al-doped Si, the relative difference does not exceed 20%. Nevertheless, both simulation results do not fit satisfyingly to the experimental data. Especially they lead to broadly underestimated saturation current densities for non-passivated Al-p^+ surfaces.

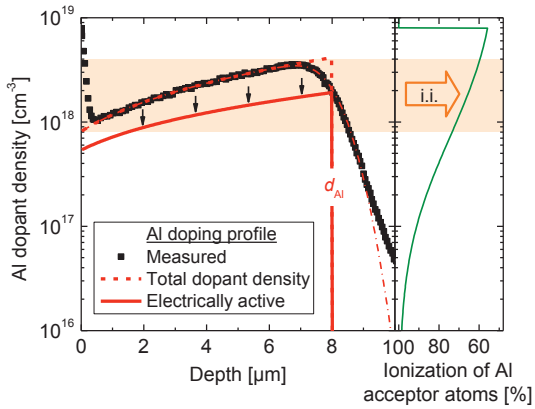

Fig. 2. Al doping profile measured by ECV (squares). At the interface of the Al-doped p^+ Si and the Si bulk, the profile is broadly blurred due to lateral thickness inhomogeneities of the Al-p^+ region. The measured data were fitted (dash dotted) with a convolution of a Gaussian distribution, representing the thickness deviations, and an abrupt doping profile (dashed) [16]. Due to incomplete ionization (i.i.) of the Al atoms (right), the resulting electrically active dopant concentration (line, left) is significantly decreased.

4. Incomplete ionization of acceptor atoms

Incomplete ionization (i.i.) can significantly affect the electrically active concentration of Al acceptors in Si within the doping range of 10^{17} to 10^{19} cm^{-3}, relevant for the profiles discussed in this work [23]. As has been reported in Refs. [27, 28], the ionization energy $E_{\mathrm{dop},0} = 69$ meV of Al [29] is much higher than those of boron acceptors (44 meV) or phosphorus donors (46 meV). Consequently, the influence of i.i. in Si is much greater for Al than for B or P dopants.

In Sentaurus TCAD [22], the predefined model for the fraction of ionized acceptor atoms $N_\mathrm{A}/N_{\mathrm{A},0}$ is given by:

$$\frac{N_\mathrm{A}}{N_{\mathrm{A},0}} = \left(1 + g_\mathrm{A}\frac{p}{p_1}\right)^{-1} \quad \text{with} \quad p_1 = N_\mathrm{V}\cdot\exp\left(-\frac{E_\mathrm{A}-E_\mathrm{V}}{k_\mathrm{B}T}\right) \quad \text{for} \quad N_\mathrm{A} < N_\mathrm{crit}. \tag{1}$$

N_V denotes the effective density of states at the edge of the valence band, E_V the upper limit of the valence band energy, k_B the Boltzmann constant and T the temperature. g_A is the inverse of the degeneracy factor $g = 1/4$, which is the convergence limit of the i.i. model proposed by Altermatt [27, 28] for low doping concentrations. In this more generalized i.i. model, as a main difference to the model implemented in Sentaurus TCAD, $g_\mathrm{A} = g_\mathrm{A}(T, N_\mathrm{A}, n, p)$ follows a functional behavior. This leads to a smooth transition to complete ionization instead of a hard transition enforced by a step function. As there are not given sufficient experimental data in literature for Al-doped Si, which serve as a firm base for this i.i. model, we have used the i.i. model implemented in Sentaurus TCAD with the default parameters [22]. $E_{\mathrm{dop},0}$ for Al-doped Si was taken from literature and a critical doping concentration N_crit for the Mott (metal-insulator) transition above 8×10^{18} cm^{-3} was used.

With N_t^* as the only free parameter in the model implemented in Sentaurus TCAD, we achieve very good agreement of measured and calculated $j_{0,\mathrm{Al}}$ values by taking i.i. into account (Fig. 3). In these calculations, a more realistic surface recombination velocity parameter $S_0 = 100$ cm/s has been assumed for passivated surfaces (open symbols) [30]. We have additionally determined an averaged SRH lifetime

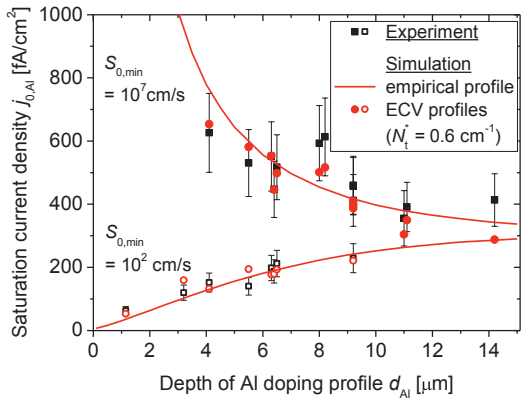

Fig. 3. Measured saturation current densities $j_{0,Al}$ of our test samples featuring non-passivated (solid squares) and passivated (open squares) Al-p^+ surfaces. Incomplete ionization of the Al acceptors has been taken into account, additionally to Auger and SRH recombination. The simulation results are shown for calculations using (a) the empirical profiles (line) described in section 2 or (b) the corresponding deconvoluted fits to the measured Al profiles (solid and open circles), exemplarily shown in Fig. 2.

in the Al-p^+ region of $\bar{\tau}_{SRH} = 270$ ns by using the SRH model with $N_t^* = 0.6$ cm^{-1} (Fig. 3), being in good agreement to results reported in Ref. [31] ($\bar{\tau}_{SRH} \geq 130$ ns).

5. Conclusions

In this study we have introduced an advanced method for accurate modeling of highly Al-doped Si. We have compared the influence of different defect models on the saturation current densities of Al-p^+ regions and have analyzed incomplete ionization of the Al acceptors in detail. The simulation results have been validated within a broad range of experimental data. Defect recombination in highly Al-doped Si has been identified to be the major loss mechanism. However, due to a much higher ionization energy compared to other acceptor atoms, as for example boron, incomplete ionization significantly impacts the saturation current densities. This is due to a major decrease of the electrically active Al concentration in the range of $N_A = 10^{17}$ to 10^{19} cm^{-3}. Taking this effect into account, we have achieved very good agreement of measured and calculated $j_{0,Al}$ values. This leads to the conclusion that incomplete ionization in combination with Auger and SRH recombination has to be accounted for in accurate modeling of highly Al-doped Si.

Acknowledgements

The authors would like to thank Gergö Létay and Stefan Odermatt from Synopsys for their support and Martin Bivour, Bernhard Michl, Christian Reichel and all other colleagues at Fraunhofer ISE for fruitful discussions.

References

[1] Rüdiger M, Schmiga C, Rauer M, Hermle M and Glunz SW, Proc. 25th EU PVSEC, Valencia, Spain, p. 2280-6 (2010).
[2] Schmiga C, Nagel H and Schmidt J, Progress in Photovoltaics: Research and Applications **14**, p. 533-9 (2006).

[3] Schmiga C, Rauer M, Rüdiger M, Meyer K, Lossen J, Krokoszinski H-J *et al.*, Proc. 25th EU PVSEC, Valencia, Spain, p. 1163-8 (2010).
[4] Hacke P, Moschner J, Yamanaka S and Meier DL, Proc. 19th EU PVSEC, Paris, p. 1292 (2004).
[5] Mihailetchi VD, Sainova DS, Geerligs LJ and Weeber AW, Proc. 22nd EU PVSEC, Milan, p. 837 (2007).
[6] Bock R, Schmidt J and Brendel R, Phys. Status Solidi RRL, 2, 6, p. 248 (2008).
[7] Schutz-Kuchly T, Veschetti Y, Cabal R, Sanzone V and Heslinga D, Proc. 24th EU PVSEC, Hamburg, p. 955 (2009).
[8] Kopecek R, Halm A, Popescu L, Peter K and Vázquez MA, Proc. 35th IEEE PVSC, Honolulu, p. 001423 (2010).
[9] Gong C, Singh S, Robbelein J, Posthuma N, Kerschaver Ev, Poortmans J and Mertens R, Progress in Photovoltaics, DOI: 10.1002/pip.1035 (2010).
[10] Clugston DA. and Basore PA, Proc. 26th IEEE PVSC, Anaheim, USA p. 207-10 (1997).
[11] Altermatt PP, Steingrube S, Yang Y, Sprodowski C, Dezhdar T, Koc S, Veith B, Herrman S, Bock R, Bothe K, Schmidt J and Brendel R, Proc. 24th EU PVSEC, Hamburg, Germany, p. 901-6 (2009).
[12] Davis JR, Rohatgi A, Hopkins RH, Blais PD, Rai-Choudhury P, Mccormick JR *et al.*, IEEE T-ED, Vol. ED-27, No. **4**, 1980.
[13] Rosenits P, Roth T, Glunz SW and Beljakowa S, Appl. Phys. Lett. **91**, 122109 (2007), erratum for σ_e value will be published.
[14] Schmidt J, Appl. Phys. Lett. **82** (13), 2178-80 (2003).
[15] Marchand RL and Sah C-T, J. Appl. Phys., **48** (1), 336-41, (1977).
[16] Shockley W and Read WTJ, Phys. Rev. **87**, 835 (1952).
[17] Hall RN, Phys. Rev. **87**, 387 (1952).
[18] Rauer M, Schmiga C, Hermle M and Glunz SW, Physica Status Solidi A 1-3 (2009).
[19] Rauer M, Schmiga C, Hermle M and Glunz SW, Proc. 24th EU PVSEC, Hamburg, Germany, p. 1059-62 (2009).
[20] Kane DE and Swanson RM, Proc. 18th IEEE PVSC, Las Vegas, USA, p. 578-83 (1985).
[21] Sinton RA, Cuevas A and Stuckings M, Proc. 25th IEEE PVSC, Washington DC, USA, p. 457-460 (1996).
[22] Sentaurus TCAD, release E-2010.12.
[23] Huster F and Schubert G, Proc. 20th EU PVSEC, Barcelona, Spain, p. 1462-5 (2005).
[24] Altermatt PP, Schenk A, Geelhaar F and Heiser G, J. Appl. Phys. **93** (3), pp.1598-1604 (2003).
[25] Misiakos K and Tsamakis D, J. Appl. Phys. **74** (5), 3293-7 (1993).
[26] Bock R, Altermatt PP, Schmidt J and Brendel R, Semicond. Sci. Technol. **25**, 105007 (2010).
[27] Altermatt PP, Schenk A and Heiser G, J. Appl. Phys. **100**, 113714 (2006).
[28] Altermatt PP, Schenk A, Schmithüsen B and Heiser G, J. Appl. Phys. **100**, 113715 (2006).
[29] Fischer DW and Rome JJ, Phys. Rev. B **27**, 4826 (1983).
[30] Hoex B, Schmidt J, Bock R, Altermatt PP, van de Sanden MCM and Kessels WMM, J. Appl. Phys. **91**, 112107 (2007).
[31] Schmidt J, Thiemann N, Bock R and Brendel R, J. Appl. Phys. **106**, 093707 (2009).